The Journal of Korea Vacuum Science & Technology
Vol. 3, No. 1, April 1999, pp. 1~9

Phenomenological monte carlo simulation model for predicting B, BF_2, As, P and Si implant profiles in silicon-based semiconductor device

Oh-Kuen Kwon*, Myung-Sik Son and Ho-Jung Hwang***

**Semiconductor Process and Device Laboratory,*
Dept. of Electronic Engineering, Chung-Ang University, 156-756, Korea
***Dept. of Electronic Engineering, Semyung University, 390-711, Korea*
(Received February 22, 1999)

Abstract – This paper presents a newly enhanced damage model in Monte Carlo (MC) simulation for the accurate prediction of 3-Dimensional (3D) as-implanted impurity and point defect profiles induced by ion implantation in (100) crystal silicon. An empirical electronic energy loss model for B, BF_2, As, P, and Si self implants over the wide energy range has been proposed for the ULSI device technology and development. Our model shows very good agreement with the SIMS data over the wide energy range. In the damage accumulation, we considered the self-annealing effects by introducing our proposed non-linear recombination probability function of each point defect for the computational efficiency. For the damage profiles, we compared the published RBS/channeling data with our results of phosphorus implants. Our damage model shows very reasonable agreement with the experiments for phosphorus implants.

I. Introduction

The continued scaling of feature size in the ULSI device technology has required shallower, more compact impurity profiles, and more precisely controlled doping profiles. In addition, the implant-induced damage has large effect on the impurity diffusion such as TED (Transient Enhanced Diffusion) phenomena during thermal annealing after ion implantation. Detailed understanding is needed of dependence of both the impurity and the damage profiles on all of the key implant parameters such as energy, dose, tilt and rotation of the wafer. Simulation of subsequent thermal processing (diffusion models) must begin with the correct as-implanted impurity and the damage profiles. As a result, greatly reduced thermal budgets are necessary for the development and manufacturing of VLSI and ULSI CMOS devices. For this reason, the final dopant profile after heat treatments depends more strongly on the as-implanted impurity and the defect profiles, and an accurate and efficient physically based 3D model capable of predicting the as-implanted dopant and the defect profiles around and under the implanted area becomes highly desirable.

In this paper is presented a newly enhanced 3D Monte Carlo (MC) damage model for the dynamic simulation in order to accurately and consistently predict the implant-induced point defect distributions of various ions in crystalline silicon. This model was applied to B, BF_2, As, P, and Si self implants over the wide energy range for the ULSI silicon-based device technology and development. The 3D trajectory split method [1], the shadow ion approach [2], and the dose split algorithm [3] related to the cumulative damage effect have been implemented into our model to get the computationally efficiency and reduce the statistical fluctuations of the implanted impurity and the defect profiles in the relatively large implanted area as compared to 1D or 2D simulations.

Also, an empirical electronic energy loss model is proposed for B, BF_2, As, P, and Si implants for the simulations over the wide energy range from few keV to several MeV.

In addition, we proposed the non-linear recombination probability function based on each local point defect concentration in order to consider the self-annealing effect for the accumulation of the point defects during the room-temperature implants. The model shows very good agreement with the published SIMS data [4-6] over the wide energy and dose range. We achieved very reasonable agreement with the RBS/channeling damage profiles [3].

This model, TRICSI (TRansport Ions into Crystal-Silicon), can predict accurately the 3D formations of amorphous regions and the ultra-shallow junction around the implanted region

II. Empirical Electronic Energy Loss Model in (100) Single-crystal Silicon

It consists of nonlocal part that is proportional to the flight-path length, and an impact parameter dependent part similar to the Hobler's model [7]. Our difference exists in the local model. The local model is used the modified Firsov Model [8] instead of the Oen-Robin model [7]. Our model takes the below equation form, where the non-local energy loss ΔE_{nl}^{LSS} is the LSS model, and ΔE_{loc}^{Morris} is the Morris model. The f_{nl} factor determines the ratio of non-local energy loss to local energy loss. We introduce the K_H correction factor for high-energy implants. The K_H increases gradually by the K_{ion} and K_{ion} factors related to the relative velocity term v/v_B, where the v is ion velocity and the v_B is Bohr velocity. The *max* function always chooses the K_H greater than 1. In the Morris Model, we set the transition critical velocity $v_{crit} = v_B Z_1^{2/3}$ [8] between high-energy equation and low-energy equation.

$$\Delta E_{el}^{total} = K_H \cdot [(1 - f_{nl}) \cdot \Delta E_{loc}^{Morris} + \Delta E_{nl}^{LSS}]$$

$$K_H = max\left(\left(K_{ion} \cdot \frac{v}{v_B}\right)^{K_{ion}},\ 1.0\right) \quad (1)$$

We used the same factors for phosphorus and silicon implants in the electronic energy loss model. This is why the impurity profiles of silicon self implants cannot be directly measured by SIMS. However, the mass and atomic number of silicon are very close to those of phosphorus. Therefore, the impurity profiles of silicon and phosphorus should be very close for the same implant conditions. We show this results in the Fig. 1(a) for the comparison of silicon self implants and phosphorus implants with the phosphorus SIMS experiments at the same implant conditions. Our model for phosphorus implant shows very good agreements with the SIMS data over the wide energy range up to 2.9 MeV as shown in the Fig. 1(b). Therefore, the silicon self implants and the silicon recoils can be simulated with the same factors of phosphorus implant. The parameters related to our electronic loss model are summarized and listed in the Table 1.

III. Details of Dynamic Damage Model for 3D Ion Implantation Simulations

In our results for point defects, the point defect distributions are much less than those of the modified Kinchin-Pease approach. We found that the reduction factor due to self-annealing effect in the

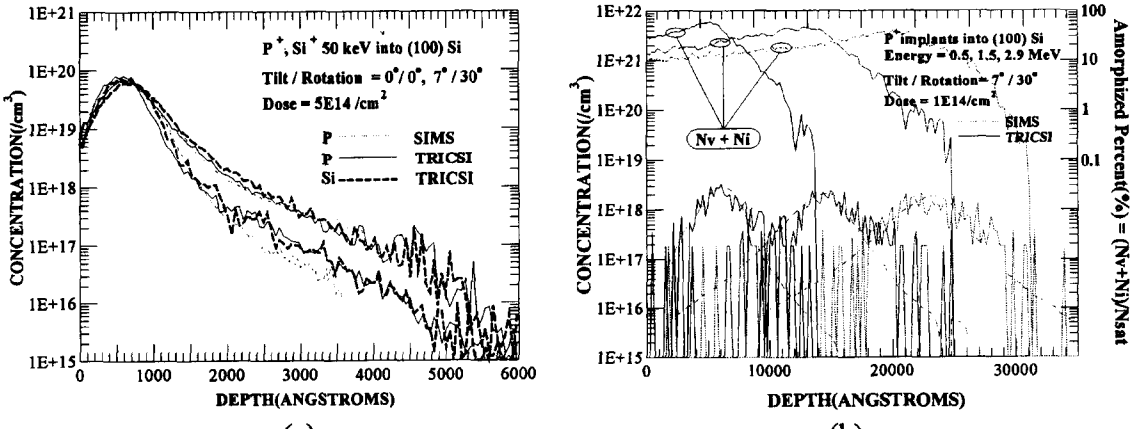

Fig. 1. Illustration of the ability of TRICSI to accurately simulate the tilt/rotation dependence of both P and Si implants into (100) Silicon compared with the SIMS experiments.
(a) TRICSI results of Si self implants and P implants into (100) Si at 50 keV, 5×10^{14} cm^{-2} dose, (b) The as-implanted impurity and the calculated amorphized percent defined by $(N_v+N_i)/N_{sat}$ of P implants into (100) Si at 0.5 to 2.9 MeV.

Table 1. The parameters related to our electronic energy loss model for B, BF_2, As, P, Si implants in silicon: k/k_L (correction factor to the Lindhard model), f_{nl} (nonlocal fraction), and a/a_M (ratio of the screening length in our model with respect to the Moliere screening length). E denotes the ion energy in eV

Ion	a/a_M	f_{nl}	k/k_L	K_{ion}	k_{ion}	Verified E Range
P, Si	0.55	$0.25\ (E/eV)^{0.05}$	1.5	2.0	0.6	15 keV ~ 2.9 MeV
As	0.70	0.1	1.0	1.0	0.0	15 keV ~ 180 keV
B, F	0.40	$0.16\ (E/eV)^{0.12}$	1.5	1.0	0.5	15 keV ~ 380 keV

result of the Kinchin-Pease approach is varied for different ions and various energies. This fact is not desirable for the physical consistency. Therefore, we calculated the trajectories of both ions and recoils. The defects generated in the collisions are saved at the local unit volume. After finishing the calculation of one particle trajectory, the defect recombination with the previous defects is always checked by using the recombination probability of each defect such as vacancy, self-interstitial, and impurity. For the dechanneling of the moving particles due to the presence of the damage, there are three dechanneling cases in our model. One is the motion in the presence of the point defects, and the other is the dechanneling in the amorphous pockets before the formation of the completely amorphized regions. In the amorphized local region, we used the TRIM model for the dechanneling process. The mesh detection for the dechanneling process in the collision phase was not applied for computational efficiency in this model. This process in the simulation is so time-consuming that we used the following idea. Our idea is that if the flight-path length between two collisions is over the local boundary, that is, several 3D cells are detected, the point defects of the local cells are averaged. Therefore, the damage parameters for the dechanneling process in this model are greater than Hobler's, Yang's and Posselt's model [7-9].

We have proposed a new recombination probability function proportional to the existing defect concentration in the local region to consider the self-annealing effect in the damage accumulation. It models the quantitative non-linear accumulation of damage during ion implants. Our insights for the damage build-up is as the followings. The point defects are likely to form clusters and amorphous pockets in the local region. In these cases of clustering and forming of amorphous pockets, the damage distribution is not uniform, and thus the recombination probability is not linearly increased proportional to the defects. Our assumption is unlike those of the reference [4] and [7], even though they used the reduction factor proportional to the defect concentration for the self-annealing recombination. Due to the defect clusters and amorphous pockets, the short-time recombination process mainly due to the migrations of the isolated defects or freely mobile defects may decrease non-linearly with the damage growing. This is very reasonable assumption because, for typical cascades, the isolated defects are more quickly recombined with other defects or forms defect clusters in damaged regions. The damaged regions overlapped and extended to form very stable amorphous pockets at the room temperature. In the highly disordered region or amorphous pockets, the recombination rate should be smaller than any same isolated and uniformly distributed defects. These insights incorporated in modeling the self-annealing process combined with the statistical dechanneling process of moving atoms during ion implants.

The self-annealing phase of the defect recombination happens shortly after displacement cascade and lasts until the next ion comes to the same damage region. This period lasts for 0.1 milliseconds or longer for typical dose rates [9-10]. These processes [9-10] are very complicate and not well defined within the binary collision approximation (BCA) framework when the defect migration and recombination related to the dose rate (ion beam current) are considered. At constant temperatures and low dose rates, both parameters depend only on ion mass, that is, on the morphology of the created damage. Thus, we did not include the dose rate effect for the recombination of point defects. Only due to the self-annealing, the point defect recombination process during ion implantation at room temper-

ature is defined by introducing the simple formula, which resulted in the saturation concentration N_{sat} for the point defects, not like the amorphized threshold concentration N_a in the reference [4].

We defined the defect saturation concentration $N_{sat} = N_v + N_i$ in the completely amorphized regions, where the N_v is the vacancy concentration and the N_i is the interstitial concentration in the local cell. It was set to 20% of the silicon density N_{si} of $5\times10^{22}/cm^3$ in our simulations. In the amorphized and defect-saturated regions the recombination probability for the vacancy and the interstitial should be 0.5 if the vacancies are equal to the interstitials [7]. The 0.5 probability at the saturation density comes from the fact that the probability for recombination $P_{ri} = P_{rv}$ defined in the below equation [2] should be equal to the survival probability 1- P_{ri} = 1-P_{rv}, assuming $N_v = N_i$. The P_{ri} or P_{rv} results in the elimination of a pre-existing point defect, and the 1- P_{ri} or 1-P_{rv} results in the addition of a point defect. Thus, the defects may saturate in this region. These results lead to the recombination probability 0.5 for each defect at the saturation density. Similarly, the defect threshold concentration N_a for amorphization or each defect saturation concentration is half of N_{sat}, that is, 10% of the silicon density N_{si} in our model [3-4].

Generally, the difference of the quantity between the interstitial and the vacancy at the same range is very small for low-energy implants. This is because in the low-energy implants the secondary ion's path is shorter than the ion's path. However, the high-energy implants are not likely to the low-energy case. The energy transferred to the lattice silicon atom are higher and the range for the recoiled silicon is longer. The moving ion's momentum transfers to the target atom are more likely for the self-interstitial to exist at deeper silicon bulk than vacancy production. In this point of view, vacancy-interstitial or interstitial-vacancy recombination should be treated separately for the accurate defect accumulation. In our model, the locations of the vacancy and the interstitial are not recorded. But, we treats the damage components separately, which are the vacancy and the interstitial. Therefore, we can distinguish the collision with vacancy or the interstitial by each dechanneling probability defined in the below equations related to the dechanneling processes of ion motion. This makes the defects create statistically in our modeling.

The recombination probability P_{rv} for vacancy recombination based on the pre-existing interstitial concentration and the interstitial recombination probability P_{ri} based on the pre-existing vacancy concentration are defined as the following formula, where N_v and N_i are the survived interstitial and the previously created vacancy concentrations in the local volume, respectively.

$$P_{rv} = k_{rv}\left(\frac{2N_i}{N_{sat}}\right)^{r_v},\ P_{ri} = k_{ri}\left(\frac{2N_v}{N_{sat}}\right)^{r_i} \qquad (2)$$

The r_i and r_v factors describe the non-linear property for the complicate short-time recombination process, and the defect recombination efficiency decreases with growing the damage. The k_{rv} and k_{ri} factors imply that each defect saturates in the amorphized region. These set to the same factor 0.5 to reflect the recombination probability at the defect saturation density. After the completion of each cascade for ions and recoils, the vacancy-interstitial recombination is checked by using the random number evenly distributed between 0 to 1 according to each above probability.

It is well known that the amorphous pockets generated by high mass ion implants, as shown by molecular dynamics (MD) calculations [10, 11], cannot be well represented within the framework of BCA/MC technique. In this damage model, the amorphous pockets or amorphous layers are modeled phenomenologically in the following ways. The whole single crystal is divided into many small 3D simulation cells. If the point defect concentration reaches a critical concentration in a particular cell, then this cell is locally and completely amorphized. After amorphization, the amorphous TRIM model [12] is used. However, the electronic energy loss model and the interatomic potential are same with the crystal model. Only the determination of the collision length between two atoms and the random impact parameter for the collision is the same with the TRIM code. The amorphous criteria are defined as the total point defect concentration of N_v + N_i, which reached to and over the saturation concentration N_{sat} of the point defect. In this region, the damage percentage P_d defined in the below equation [3] is 100% and the defect generation and

recombination is the same quantity, and thus defects remain constant. In this amorphous region, defect recombination is not included until moving ions and recoils are out of the region. This is due to the difficulties in defining the vacancy and the interstitial when the TRIM model is used even though this region may be over-saturated. These cells have accumulated in a series, which amorphous layers form. The damage percentage P_d in the local region is defined as the following equation (3). One consequence of the damage accumulation is its effect on the subsequently implanted ions. The damage can block the channeling motion of the ions and change their destination. Therefore, this is an essential part of damage modeling. In the present model, there are three possible dechanneling mechanisms. The damage dechanneling probability f_d due to a single interstitial, interstitial cluster, and amorphous pockets are defined as the following equation (3), where the k_d is a fine-tuned parameter for different ion implants to model the interstitial clusters.

$$P_d = \frac{N_v + N_i}{N_{sat}}, \quad f_d = k_d \cdot (1 - e^{-P_d}) \tag{3}$$

In addition, the clustering has a higher priority to happen than recombination in a damaged region. Therefore, in a highly damaged region, the defect remains as "amorphous pockets" and would not completely anneal out due to the random recombination. This priority is phenomenologically represented by introducing an amorphous pocket encountered probability P_a. This probability is introduced as fine-tune factor for each implanted species to obtain the best agreement with the experimental impurity profiles in the present model. The amorphous pockets encountered probability is defined as the following equation (4).

$$P_a = k_a \cdot f_d, \quad P_i = (1 - k_a) \cdot f_d \tag{4}$$

where the k_a is a parameter for fine-tuning the simulation results to the experiments. The value is less than 1.

In the amorphous pockets, the interstitial is created at the distance l_c to the direction of a moving atom randomly chosen according to the equation (6). The defects are assumed to be randomly distributed within the collision radius r_c in the following equation:

$$l_c = r_c \cdot R_n \tag{5}$$

where the R_n is the random number, and the r_c is a collision radius for amorphous pockets.

In our model, the maximum cluster size is not defined, and thus the cluster size is randomly determined when a series of interstitials is determined by a series of random numbers.

The single interstitial encountered probability *Pi* is defined in the above equation (4). If a single interstitial is encountered, the interstitial is placed in the random configuration on the flight-path length *FPL* between two collisions. The length *FPL* is first searched in the ideal crystal structure. After that, the interstitials are created at the length l_c on this path *FPL* by using the random number like the below equation (6). The function *max* chooses the collision length greater than the minimal single interstitial location r_{min} on the ideal path *FPL*. At the distance l_c from the point of the previous collision, a single interstitial is created.

$$l_c = max((FPL - r_{min}) \cdot R_n + r_{min},\ r_{min}) \tag{6}$$

Finally, if an amorphous region is encountered, the projectile is assumed to travel in an amorphous silicon like the TRIM model (12) until it is out of this region.

After failing in searching the interstitial or interstitial clusters or the amorphized regions described above, a vacancy location at the silicon lattice site is checked whether the collided silicon position with the moving projectile or recoiled atoms is occupied by a vacancy or not. The vacancy encountered probability P_v is defined as the following equation:

$$P_v = k_v \cdot \left(\frac{2N_v}{N_{sat}}\right) \tag{7}$$

The k_v factor models the clustering behavior according to the implanted ion's mass. The vacancy tends to recombine quickly with the interstitial. During the ion implants, the vacancies form clusters like the interstitials. However, vacancy clustering does not enhance the channeling process more significantly in ion motion than interstitial clustering. This is because the vacancies are surrounded interstitials in highly disordered regions or amorphous pockets, and the

vacancy migration for recombination in this amorphized region is diminished as the damage grows up. [3] Therefore, we used the equation (7) as the vacancy encountered probability to consider the vacancy clustering effect in the dechanneling process.

IV. Simulation Results

For silicon self implants, the impurity profiles cannot be directly measured by SIMS. However, the mass and atomic number are very close to phosphorus, and thus, the impurity profiles of silicon and phosphorus should be very close for the same implant conditions. We show this result in the Fig. 1(a) for the comparison of silicon self implants and phosphorus implants with the phosphorus SIMS experiments [3] at the same implant conditions. The implant conditions are included in the figures. It can be seen that the agreement between simulation and experiment are very good. Therefore, the impurity profiles of silicon self implants can be simulated with the same phosphorus parameters related to the damage accumulation and the electronic energy loss.

In the Fig. 1(b), we show the results of phosphorus implants over 500 keV to 2.9 MeV are presented for the as-implanted impurity and the calculated amorphized percent defined by $(N_v+N_i)/N_{sat}$. The good agreement with the SIMS data [2] is achieved.

In order to verify the simulation results for the point defect distribution as shown in the Fig. 2(a), we show the tilt/rotation angle dependence of the damage profiles for phosphorus implants into (100) Si at an energy 50 keV and a dose $2\times10^{15}/cm^2$. It is seen that the TRICSI with the new damage model and electronic energy loss model can predict well the damage profiles. It is noted that in these experiments taken from the reference [3], the flat tails are due to RBS background noise, and hence should be ignored. The defects over 100% in our simulation results are due to the additional implanted impurity interstitials. We always check the impurity recombination as a substitutional with the vacancies and then, the survival impurity added to the total defects. The 100% defect concentration previously defined N_{sat} is $1\times10^{22}/cm^3$.

The amorphization threshold dose for phosphorus in our calculations is about $3\times10^{14}/cm^2$ and our calculated amorphized thickness' are compared with the RBS/channeling experiments [3] as shown in the Fig. 2(b). The simulation results show that before 100 keV, our results are very good agreements with the experiments, however, after higher energies, the

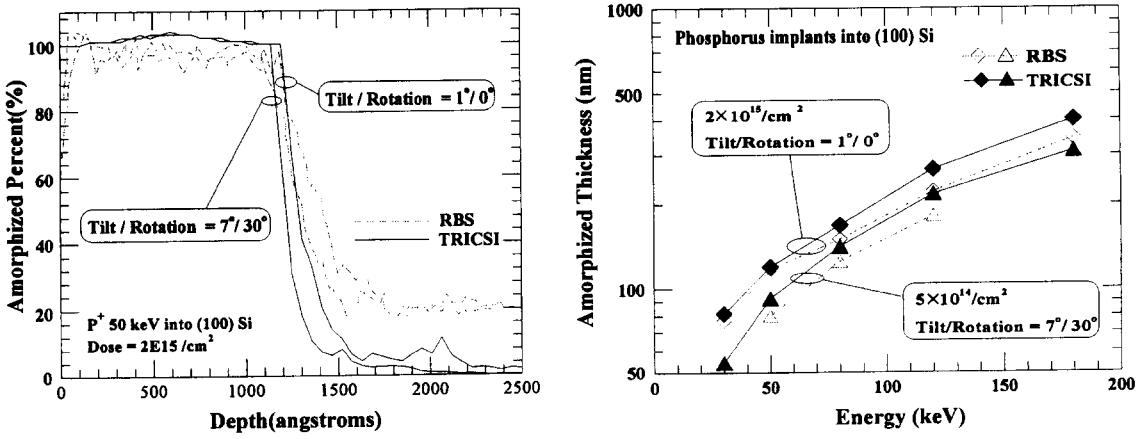

Fig. 2. Illustration of the ability of TRICSI to accurately simulate the P-induced damage profiles compared with the RBS/channeling experiments.
(a) Comparison TRICSI results with RBS/channeling experiments of P implants into (100) Si at an energy 50 keV, 2×10^{15} cm^{-2} dose, (b) The tilt/rotation angle dependence of the damage profiles for P implants into (100) Si at the different energy range and doses.

deviations are occurred. We believed that this is because our simulations for these results do not consider the after-implant annealing process at room temperature and the dose-rate related self-annealing process. Our modeling for the self-annealing effect is confined to the statistical and phenomenological model at the room-temperature implants. In our results for each point defect as shown in the Fig. 1 and 2, the point defect distributions are much less than those of the modified Kinchin-Pease approach [12]. This is because the Kinchin-Pease equation does not consider the crystal structure and the self-annealing effect between the vacancy and interstitial at room temperature.

The SIMS data for the comparison with the simulation results are taken from the references [4-6]. Our full-dynamic damage model predicts well the As, B, and BF_2 impurity range profiles dependent

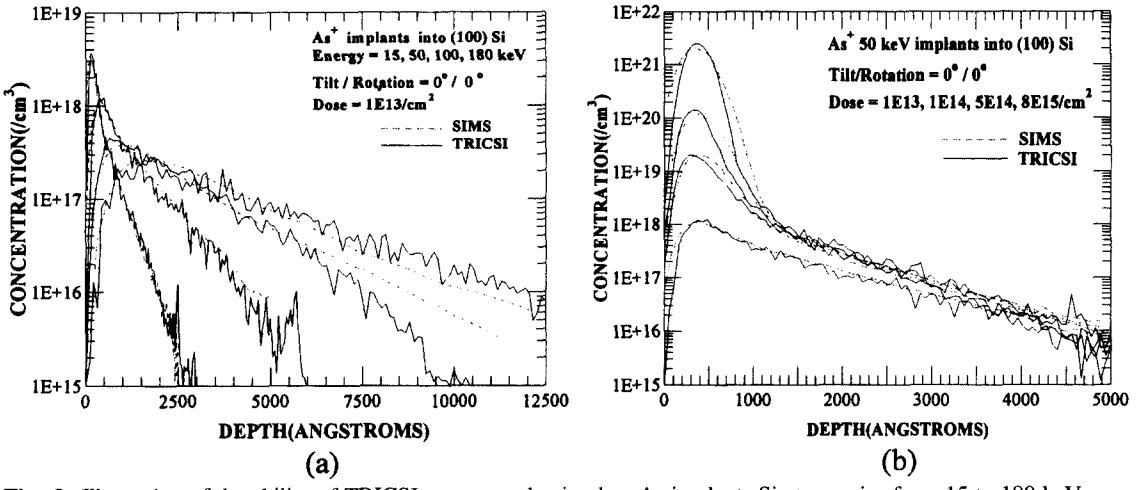

Fig. 3. Illustration of the ability of TRICSI to accurately simulate As implants Si at energies from 15 to 180 keV compared with the SIMS experiments.
(a) Our full-dynamic damage model results of As implants into (100) Si at the different energy range, 1×10^{13} cm^{-2} dose,
(b) Our full-dynamic damage model results of As implants into (100) Si at the different dose range, 50 keV energy.

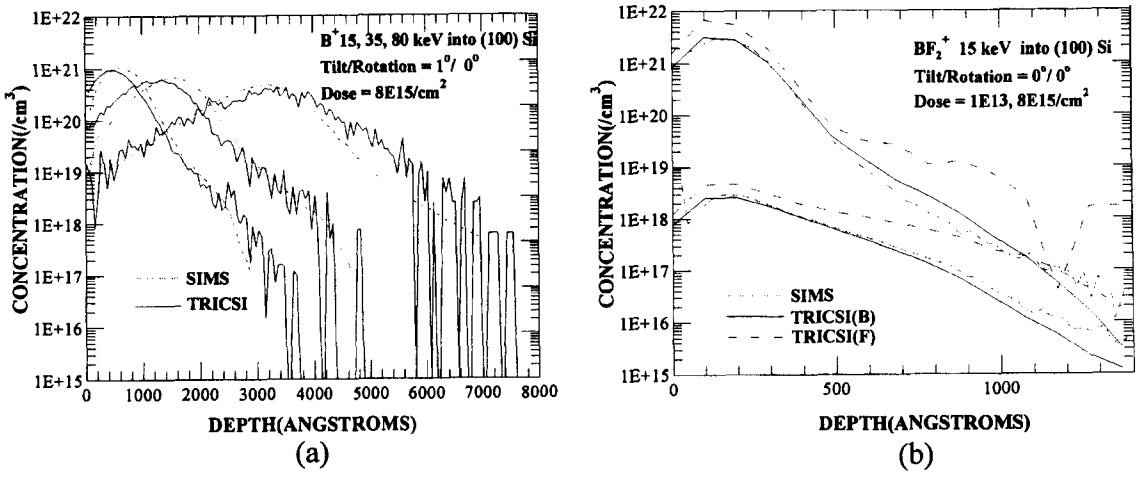

Fig. 4. Illustration of the ability of TRICSI to accurately simulate B and BF2 implants into (100) Silicon at energies from 15 to 85 keV compared with the SIMS experiments.
(a) Our full-dynamic damage model results of B implants into (100) Si at the different energy range, 8×10^{15} cm^{-2} dose,
(b) Our full-dynamic damage model results of BF_2 implants into (100) Si at the different dose range, 15 keV energy.

on the various doses, energies and tilt and rotation angle as shown in the Fig. 3 and 4.

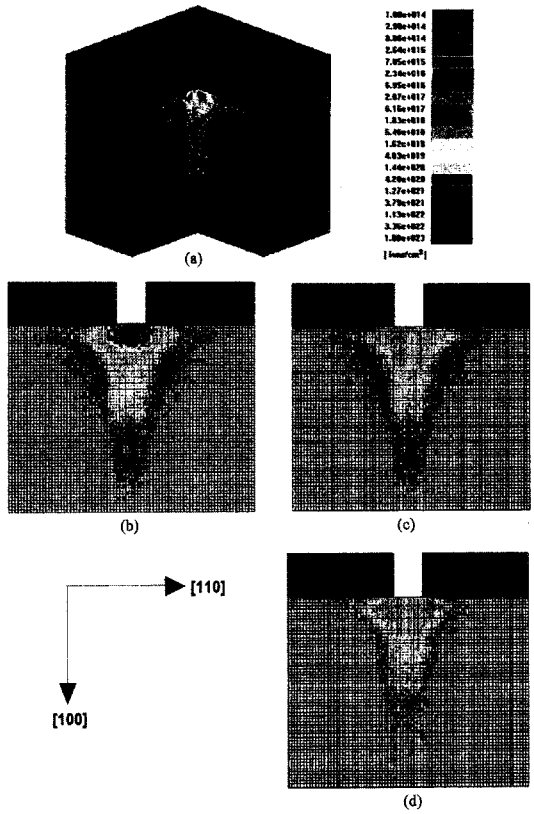

Fig. 5. Illustration of the capability of TRICSI for the 3D as-implanted impurity and damage profiles to accurately simulate P implants into (100) Silicon at energy 30 keV, dose $1\times10^{16}/cm^2$, 0° tilt and 0° rotation angles.
(a) 1/4 section view of the 3D P impurity profile, (b) 1/2 section view of the 3D P-generated damage profiles, (c) 1/2 section view of the 3D P-generated imterstitial profile, (d) 1/2 section view of the 3D P-generated vacancy profile.

Finally, the 3D impurity and the damage profiles for phosphorus implant at 30 keV, dose $1\times10^{16}/cm^2$, 0° tilt and 0° rotation angle are presented in the Fig. 5. The figures show the 2D and 3D phosphorus impurity concentration profiles and phosphorus-generated damage profiles. The split branches were 3, split lines were 6 and the initial simulation particles were 10,000 ions. In addition, the shadow ions are applied to the initial 5% of the total simulation ions. The shadow ions are eleven times the initial 5% ions, that is, 5,500 ions to simulate for the dose $5\times10^{14}/cm^2$. The mesh volume is used 108.6×108.6×108.6 $Å^3$. The implant open area is 1086×1086 $Å^2$. The implanted volume is 4344×4344×6516 $Å^3$. The final stopped particles in the silicon bulk were 1,032,053.

In the Fig. 5(a), we show the 3D phosphorus impurity profiles in the 1/4-section view. Our model reproduces well the 3D profiles under and around the implanted area. We found these results show the round-shape concentration profiles under the implanted rectangular area if the implanted energy is high and the implanted area is relatively small. In addition, the damage accumulation becomes higher, and the lateral deviation from the mask edges becomes higher. We believe that this is because the dechanneling becomes enhanced as the damage accumulation increases, and thus the 2D lateral ranges of the implanted ions and its generating damage becomes wider.

In the Fig. 5(b), we show the 3D phosphorus-generated damage profiles. This figure shows well the 3D amorphized regions under and around the implanted area. The damage shape is similar to the impurity profiles. In the Fig. 5(b), the white circled

Table 2. The parameters related to the our damage model for B, BF_2, As, P, Si implants

Parameters \ Ions	B	BF_2 (B, F)	As	P, Si
damage dechanneling parameter k_d	0.80	0.85	0.85	0.85
amorphous pocket encountering parameter ka	0.35	0.45	0.60	0.55
recombination parameter $k_{rv} = k_{ri}$	0.50	0.50	0.50	0.50
recombination parameter $r_v = r_i$	1.00	1.20	1.33	1.20
collision radius rc factor for amorphous pocket (silicon constant unit)	0.55	0.55	0.80	0.55
minimum collision radius factor rmin for single interstitial (silicon constant unit)	0.24	0.24	0.24	0.24
vacancy clustering parameter k_v	0.10	0.10	0.20	0.10

cells indicates the completely amorphized regions and the color concentrations in this figure represent the N_v+N_i.

In the Fig. 5(c) and 5(d), we show the phosphorus-generated interstitial and vacancy concentration profiles. Our simulations treated separately interstitial and vacancy even though we did not record the exact stopped position for interstitials and the vacant position for vacancies described above sections. Our code predicts well the point defect concentration profiles. This information is presented the next thermal simulation steps in the continuous 3D process simulation. This figure indicates that the vacancy regions are smaller than those of interstitials. This is because the interstitial are more directed into the bulk at the collision event than the vacancy is frozen at the silicon lattice site. This implant feature is well presented in the simulation results.

In fact, the computation time for the 3D simulations was still very intensive in our model. The efficient simulations are not made in our paper. This is because our modeling is focused on the accuracy for the as-implanted impurity and damage profiles.

V. Conclusions

Our model does not use the exact point defect location for the calculation efficiency. Thorough the statistical creation for interstitials and vacancies, we achieved the fairly good reproducibility for the SIMS data and the reasonable agreement with the RBS/channeling damage profiles. The result of ion implants into (100) crystal silicon shows the good accuracy. The 3D dopant range profile and 3D formations of the amorphous region and the ultra-shallow junction for the ULSI device technology and development could be predicted using our model. Our quantitative damage information could be presented to the next thermal process simulations such as TED, multiple implants, and thermal diffusion.

Acknowledgement

This work was partly supported by the Korea Science and Engineering Foundation (KOSEF) under the research number 981-0907-028-2.

References

[1] M.-S. Son and H. J. Hwang, Journal of the Institute of Electronics Engineers of Korea, **35-D**, no. 3, 28 (1998).

[2] S. Tian, S. J. Morris, M. Morris, B. Obradovic, and A. F. Tasch, IEDM, Tech. Dig., pp. 713 (1996).

[3] S. Tian, Ph. D. Thesis, The University of Texas at Austin (1997).

[4] G. Wang, Master's Thesis, The University of Texas at Austin (1997).

[5] K. M. Klein, C. Park, and A. F. Tasch, Nucl. Inst. and Meth. B **59/60**, pp. 60 (1991).

[6] S.-H. Yang, C. M. Snell, S. J. Morris, S. Tian, K. Parab, B. Obradovich, M. Morris, and A. F. Tasch, J. Electrochem. Soc., Vol. **143**, no. 11, 3784 (1996).

[7] G. Hobler, Nucl. Inst. Meth. B. Vol. **96**, 155 (1995).

[8] S. J. Morris, B. Obradovic, S.-H. Yang and A. F. Tasch, IEDM, Tech. Dig., pp. 721 (1996).

[9] M. Posselt, B. Schmidt, C. S. Murthy, T. Feudal, and K. Suzuki, J. Electrochem. Soc., Vol. **144**, no. 4, 1495 (1997).

[10] T. Diaz de la Rubia and G. H. Gilmer, Phys. Rev. Lett. Vol. **74**, no. 13, 2507 (1995).

[11] M.-J. Caturla, T. Diaz de la Rubia, L. A. Marques and G.H. Gilmer, Phys. Rev. B, Vol. **54**, 16683 (1996).

[12] J. F. Ziegler and J. P. Biersack, *The stopping and Range of Ions in Solids*, Vol. I, pp. 233-263, New York: Pergamon (1985).